NJC

ROYAL SOCIETY OF CHEMISTRY

PAPER

View Article Online
View Journal | View Issue

Cite this: *New J. Chem.*, 2023, **47**, 11903

A preparation strategy for multicolor carbon dots embedded in silicone for latent fingermarks and detection of AcO^-†

Tingzhong Li,[a] Qinglu Yu,[b] Zhuang Du,[c] Jie Gao,[c] Dong LU,[d] Rui Liang*[e] and Guoxing Sun*[ab]

A convenient and mild method for preparing multicolor carbon dots (CDs) using the solvothermal process and extraction has been developed. After doping CDs as the cross-linking agent into γ-(2,3-epoxypropoxy)propytrimethoxysilane solution, orange, yellow, and blue emitting powders were fabricated, which effectively avoid aggregation-caused quenching and emit bright luminescence. By introducing oily chain segments, the interaction between the fluorescent powder and fingerprint residue is improved as well as the imaging ability of latent fingerprints. Level 1–3 features can be extracted using the CD powder developed fingerprints. Additionally, seven substrates with different surface appearance, colours, and interference were chosen to deposit on fingerprints, in which all the substrates have a good combination with the CD powder and showed excellent contrast and visibility. Notably, the as-prepared CDs can be used for acetate ion (AcO^-) sensing. The CDs exhibit an efficient response to AcO^- by an "on–off" switching strategy. As a sensing probe, the CDs exhibit a wide concentration range (3×10^{-7}–3×10^{-3} M) of response to AcO^- with a low fluorescence response threshold (0.3 μM).

Received 12th April 2023,
Accepted 18th May 2023

DOI: 10.1039/d3nj01688a

rsc.li/njc

Introduction

In recent years, there have been many reports on the analysis of latent fingerprints (LFPs). Fingerprints can be divided into three categories. Obvious and stably-formed fingerprints are directly visible, while the third category of fingerprints is invisible to the naked eye through the transfer of natural secretions (such as sweat) of the body. Even if the hands are thoroughly wiped, the LFP will still remain on the contact area. LFPs are the most common fingerprint type at crime scenes, but physical and chemical processing is required to enhance the imaging effect. Methods to enhance potential imprint imaging include optical testing, powder dusting, iodine fumigation, cyanoacrylate fumigation, ninhydrin treatment, *etc.* Therefore, the physical and chemical treatment of LFPs is essential for detection accuracy and identification. In the last decade, nano fluorescent materials (such as quantum dots,[1,2] upconversion nanomaterials,[3,4] traditional organic fluorescent dyes,[5,6] aggregation-induced emission (AIE) dyes,[7] carbon dots, *etc.*) have provided lots of innovative ideas for the detection of LFPs due to their good optical, electronic and surface modifiable properties. These materials can be combined with fingerprint residues by designing physical or chemical adsorption protocols.

Compared with other nano fluorescent materials, carbon dots (CDs) have many advantages including excellent optical properties,[8] good water solubility, low toxicity, environmental friendliness, wide source of raw materials, low cost, and good biocompatibility. Consequently, research on CDs has developed rapidly in the past decade. Its related research has appeared in frontier fields such as display lighting,[9] detection,[10–12] agriculture[13] and medical research.[14–16] There are still many application problems and coping strategies. For example, most CDs exhibit the aggregation-caused quenching (ACQ) phenomenon. To overcome the ACQ effect, many researchers use starch,[17] silicon gel,[18–21] montmorillonite,[22] PVA,[23] organic silicon[24,25] and other materials to adsorb and disperse CDs. There is only physical adsorption between the CDs and the additives, and the binding is not firm. Some special methods, such as using organic long chains to modify the surface of CDs to prevent the aggregation of the luminous group have been explored.[26] But the obtained

[a] *Zhuhai UM Science &Technology Research Institute, Zhuhai 519031, China. E-mail: gxsun@um.edu.mo*
[b] *Joint Key Laboratory of the Ministry of Education, Institute of Applied Physics and Materials Engineering, University of Macau, Macau SAR, 999078, China*
[c] *Guangzhou Lushan New Materials Co., Ltd, Guangzhou 510640, China*
[d] *Guangzhou HKUST Fok Ying Tung Research Institute, Guangzhou 510640, China*
[e] *Department of Engineering Science, Faculty of Innovation Engineering, Macau University of Science and Technology, Macau SAR, 999078, China. E-mail: rliang@must.edu.mo*

† Electronic supplementary information (ESI) available. See DOI: https://doi.org/10.1039/d3nj01688a

CDs become completely hydrophobic. The direct preparation of CDs with the AIE phenomenon has also been studied.[27] The structure of CDs cannot be accurately characterized as small fluorescent molecules, which may cause difficulties in mechanism exploration.[28–33] Researchers can analyze the influencing factors or mechanism of fluorescence by studying CD synthesis parameters and doping element states.[8,34] However, it cannot be denied that the synthesis of CDs is simple. As a result, this field can quickly get a lot of attention and follow-up research. For example, since Fernandes and his collaborators used CDs for fingerprint development, a large number of relevant studies have emerged. According to the fingerprint structure, microscopic details are divided into three levels. Level 1 details include the overall characteristics of the fingerprint, including the shape of the fingerprint (rim, ring, arch, *etc.*), the core point (also known as the center point), and the triangle point. Level 2 details encompass the macroscopic detail features of the fingerprint ridge, which are usually divided into terminals, bifurcations, islands, and short ridges, among others. Level 3 details are the microscopic detail characteristics of the fingerprint, mainly including the shape of the ridge edge and the width of the ridge and pores. Although some literature reports discuss the specific identification of CDs on fingerprint residues, and believe that the combination of CDs and fingerprints mainly includes electrostatic interaction, hydrophobic interaction and chemical coupling,[35–38] there is a lack of in-depth research on the combination principle of CDs and fingerprints. As the precise and controllable synthesis of CDs itself is not yet possible, determining what surface groups or surface states can be carried by CDs to combine with fingerprint residues remains a difficult problem to be solved. At the same time, the advantage of simple preparation of CDs will be weakened. There are many powder dusting methods to develop fingerprints by using CDs, and most of them can only detect level 2 details.[10,23,39,40]

The greatest advantage of preparing CDs using the solvothermal method is its simplicity and convenience, but there are many side effects and cumbersome purification processes. Purification needs to go through slow dialysis (or column chromatography), rotary evaporation, and freeze-drying processes, which seriously weaken its advantages. To address these issues, this work proposes a method to separate CDs of different fluorescence wavelengths from a one-pot reaction by taking advantage of the difference of polarity (group) on the surface of CDs. This process is more suitable for industrial production because of its higher efficiency, no dialysis wastewater and lower raw material consumption. The active groups present on the surface of CDs undergo a reaction with epoxy to disperse the CDs in the silicone polymer, overcoming the ACQ phenomenon and forming covalent bonds between the CDs and silicone polymer. Furthermore, grafting long hydrophobic chains on the silicone surface achieves better adhesion with the hydrophobic components in LFPs. The entire preparation process is simple and fast, and it can easily be scaled up to more than 10 kg. At the same time, we carried out ion detection on the prepared CDs. It is found that the CDs in this work are the first reported CDs used for the fluorescence detection of AcO^-. AcO^- is a crucial cellular molecule involved in many metabolic processes and has received much attention.[41,42] The production and oxidation rate of AcO^- is often used in marine sediments as an indicator of organic decomposition.[43] Therefore, the detection of a trace amount of AcO^- is not only of great significance for biological processes, but also for environmental applications.

Experimental

Materials

Urea (99%), citric acid (99.5%), and *N*,*N*-dimethylformamide (DMF, 99.5%) were purchased from Macklin. Hexane (99%), ethanol (99.7%), EA (99.0%), methanol (99.0%), propyl alcohol (99.0%), and butanol (99.0%) were purchased from Aladdin. γ-(2,3-Epoxypropoxy)propytrimethoxysilane (KH560, 96%) and *n*-dodecyltrimethoxysilane (WD-10, 96%) were purchased from Jianshuang Chemical Technology Co., Ltd. All the materials were used as purchased without further purification.

Synthesis of b-CDs, y-CDs, and r-CDs

1 g citric acid and 2 g urea were dispersed in 10 mL DMF.[44] The mixtures were added into a Teflon-lined stainless autoclave (20 mL). Then the sealed autoclave vessels were placed into an electric oven, which was set at 230 °C and held for 1 h. Then the mixture was extracted stepwise with solvents of different polarity. Hexane was added to extract the substance with blue-violet fluorescence. Then ethyl acetate was used to extract the residues in the bottle of the previous step to obtain materials with blue-green fluorescence (denoted as b-CDs,). Yellow and orange-red CD solutions (extraction solutions were alcohol and DMF, respectively) were obtained by repeating these steps, as shown in Scheme 1, denoted as y-CDs and r-CDs, respectively.

Preparation of s-b-CDs, s-y-CDs, s-r-CDs and os-b-CDs, os-y-CDs, os-r-CDs

Take a small amount (1 wt%, 1 mL) of the CD solution obtained above and add it to water (10 g) and KH560 (10 g), and heat it at 70 °C to react until curing. After drying, the resulting material was ground and passed through a 400-mesh sieve to obtain organosilicon coated powders with different fluorescence, as shown in Scheme 1, which are labeled as s-b-CDs, s-y-CDs, and s-r-CDs, respectively. Similarly, the obtained powder (0.5 g) is added to ethanol (1.5 g) and WD-10 (0.025 g), stirred at room temperature for 3 h, filtered, dried, and ground through a 400-mesh sieve to obtain hydrophobic long chain wrapped CDs, which are labeled os-b-CDs, os-y-CDs, and os-r-CDs respectively.

Detection and imaging of LFP

All fingerprints in this paper are from male adult volunteers. The latent fingerprints are prepared by gently rubbing the forehead with fingertips and then pressing on the substrate with appropriate force. The base materials include stainless steel, glass, plastic, printing paper, corrugated paper, wood, and commodity labels commonly seen in daily life. Developing

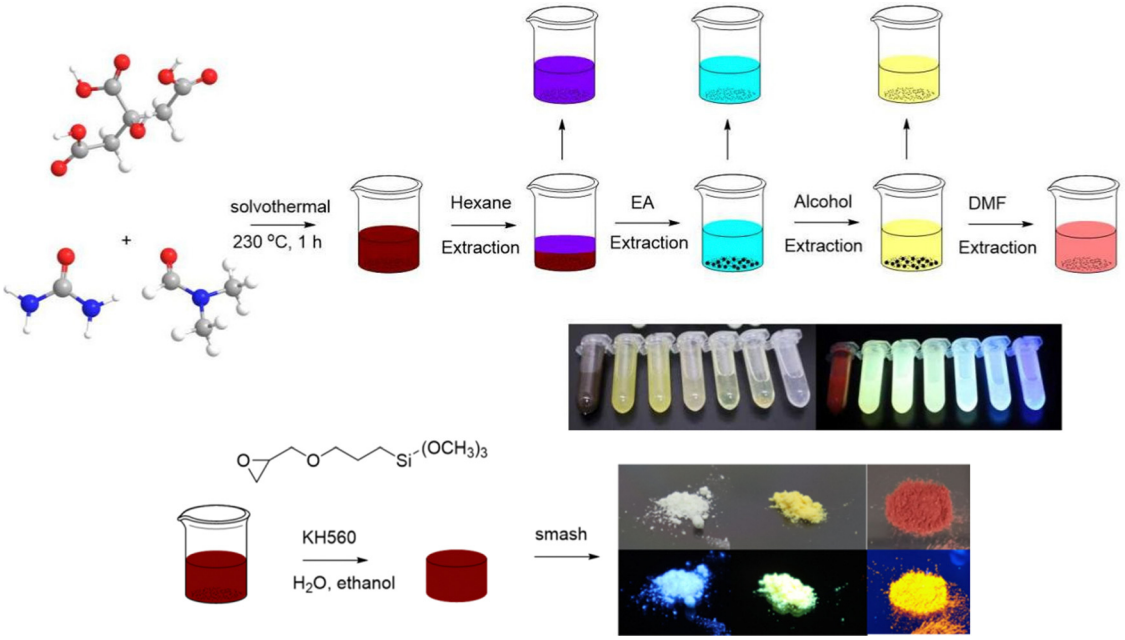

Scheme 1 Synthesis procedure of CD powders. Inset: Ambient and UV photograph of compounds in liquid (b-CDs, y-CDs, r-CDs) and solid state (s-b-CDs, s-y-CDs, s-r-CDs).

steps: apply an appropriate amount of fluorescent powder to the fingerprint brush, pat it gently above the fingerprint, and then brush the excess fluorescent powder along the fingerprint lines. Fluorescent photos were taken by a camera (Canon EOS M50) under a 365 nm UV light.

Ion detection

In a typical assay, aqueous y-CDs were mixed thoroughly with different concentrations of AcO^-. The photoluminescence (PL) spectra were collected after thoroughly mixing. The exciting and emission slits were kept constant throughout the experiment. Different ion solutions (10 mM) including Pd^{2+}, Na^+, Ca^{2+}, Al^{3+}, K^+, Cu^{2+}, Fe^{2+}, Fe^{3+}, Zn^{2+}, Mg^{2+}, Cl^-, SO_4^{2-}, NO_3^-, Br^-, I^-, and COO^-, were dropped into the aqueous CDs individually and measured in the same manner. The concentration of CDs was kept constant at 0.01 wt% for all experiments.

Results and discussion

Optical properties

As can be seen from the UV spectra (Fig. 1A), the absorption peak changes. With the increase of the polarity of the extraction solvent, an absorption peak appears at around 425 nm, followed by a new absorption peak at about 475 nm. The longer the absorption peak is, the larger the electron delocalization structure the CDs may have, which is consistent with the phenomenon that the fluorescence of the CDs changes from blue to red.[45,46] In Fig. 1B, the fluorescence of CDs separated by different polar solvents ranges from 439 nm to 615 nm. The blue-violet light substance (in Scheme 1) extracted with *n*-hexane has poor photostability, and has limited practical application value and will not be studied in this work. The b-CDs extracted by ethyl acetate have an obvious absorption peak at 350 nm, and emit 439 nm blue light. y-CDs were extracted with alcohols (methanol, ethanol, propanol or butanol) and their 350 nm absorption peak is not obvious, but new absorption occurs at 425 nm and can emit 526 nm fluorescence. The r-CDs extracted by DMF have obvious absorption and emission at 462 nm and 615 nm respectively. The fluorescence spectra of y-CD at different concentrations (Fig. 1C) show that the fluorescence emission wavelength is not affected by the concentration under the condition of good dispersion. However, the emission wavelength of CDs is significantly affected by the excitation wavelength (Fig. 1D), which is commonly found in CDs and is associated with particle sizes, various functional groups (surface states), emissive traps, conjugation structure and zig–zag sites of CDs, resulting in different excited state energy levels.[34,47,48] At the same time, as the excitation wavelength increases, the Stokes shift decreases (from 120 nm to 45 nm), and the fluorescence intensity decreases. This phenomenon is generally believed to be caused by the size of CDs. It can be seen from Fig. 1E that the fluorescence peaks of the CDs after being dispersed and wrapped with organic silicon are 434 nm, 587 nm and 660 nm respectively. After wrapping, the fluorescence wavelength of b-CDs has no obvious change, but the fluorescence wavelength of y- and r-CDs has a significant red-shift, presumably related to the change in surface states. The fluorescence quantum yield (QY) and lifetime of s-b-CDs, s-y-CDs and s-r-CDs are 27.0% (17.72 ns), 23.4% (23.87 ns) and 1.3% (14.14 ns), respectively. After embedding carbon dots into organic silicon, the photostability is significantly improved and it is resistant to fluorescence quenching by copper and iron ions (Fig. S2, ESI†). The stability of the CDs (y-CDs) *vs.* temperature, pH and different solutions has been studied in Fig. S3 and S4

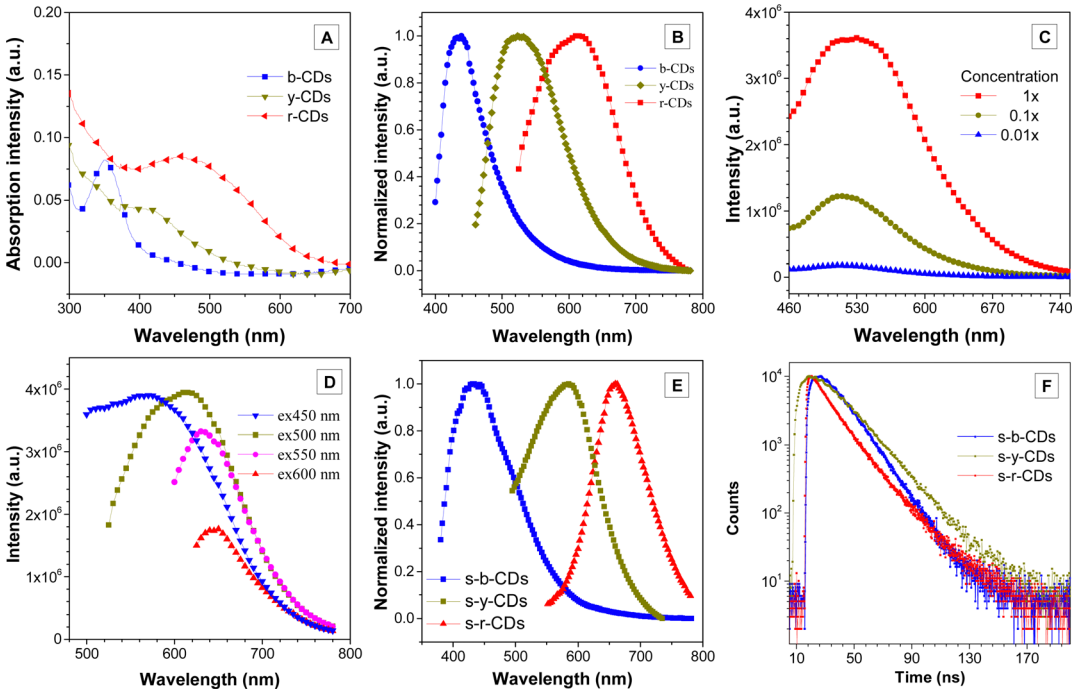

Fig. 1 Absorption (A) and emission (B) spectra of CD solution in H_2O. Emission spectra at different concentrations (C) and different excitation wavelengths (D) of y-CDs and r-CDs solution, respectively. Emission (E) and lifetime (F) spectra of s-b-CDs, s-y-CDs and s-r-CDs. CD solution concentration: 0.1 mg mL^{-1}; excitation wavelength: 351 nm (b-CDs), 360 nm (y-CDs), 500 nm (r-CDs), 365 nm (s-b-CDs), 365 nm (s-y-CDs) and 500 nm (s-r-CDs).

(ESI†). As seen in Fig. S3A (ESI†), the sample has good thermal stability in the solution state. However, under alkaline conditions, y-CDs are unstable (Fig. S3B, ESI†). After being placed at pH = 13 for 24 hours, the fluorescence shifts to 445 nm. It is speculated that part of the structure on the CDs has been hydrolyzed, as the sample does not immediately blue-shift after adding an alkaline solution, which can exclude the neutralization reaction of functional groups (such as carboxyl groups). Moreover, adjusting to neutral or acidic pH dose not restore the fluorescence wavelength.

Chemical structure and morphology characterization

Fig. S5 (ESI†) shows the infrared spectra of three fluorescent carbon dots. There should be amino and hydroxyl peaks at 3358 cm^{-1}. 1698 cm^{-1} and 1668 cm^{-1} are characteristic peaks of amide or C═N. The in-plane deformation vibrations and stretching of C–N and –OH, respectively, are shown at 1452 cm^{-1}, 1413 cm^{-1}, and 1388 cm^{-1}. Peaks at 1087 and 1049 cm^{-1} are the C–O peaks of hydroxyl or ether groups. The Fermi resonance absorption occuring between the carbonyl and α-C–H of carbonyl occurs at 881 cm^{-1}. It can be seen that the main difference between b-CDs and the other two (y-CDs, r-CDs) is the amide or C═N peak at 1668–1698 cm^{-1}, while r-CDs have a greater absorption at 1652 cm^{-1} (which should be C═C absorption) than y-CDs. The characteristic absorption peaks of Si–O–C, Si–O–Si and Si–O–H vibrations are located at 1105 cm^{-1}, 1034 cm^{-1} and 908 cm^{-1}, respectively, which suggesting the network structure of organosilicon. The exposed hydroxyl group (3465 cm^{-1}, 908 cm^{-1}) also provides the active group for the subsequent hydrophobic modification. The small absorption at 910 cm^{-1} corresponds to the presence of the epoxy group, which is catalyzed by an amine group to open the ring and react rapidly with an amine group or hydroxyl group. The absence of epoxy absorption peaks implies the presence of tertiary amines, which also catalyze the reaction of epoxy-group ring-opening with the –OH and –COOH on the surface of CDs.

To confirm the chemical composition of the CDs, and their carbon binding and nitrogen configuration, the XPS spectra of the samples were obtained. In Fig. 2(A–C), the survey spectra of b-CDs, y-CDs and r-CDs show three typical peaks at 284.8, 399.8 and 531.4 eV for C1s, N1s and O1s, respectively, which denote that no significant contaminant exists on the surface of the sample. The integral analysis of C1s, N1s, and O1s can be used to assist analysis. The carbon content in the three samples (b, y, and r-CDs) increased from 52.40% to 66.99%, while the nitrogen content decreased (from 28.68% to 13.78%), with small fluctuations observed in oxygen content. In the high resolution spectra of three samples, the C1s can be deconvoluted into five peaks (Fig. 2D, G and J), which are respectively attributed to C–C/C═C, C–N, C–O, C═O/C═N and COOH. The N1s band can be deconvoluted into four peaks corresponding to pyridinic N, amino N, pyrrolic N and graphitic N (Fig. 2E, H and K).

We all know that CDs are easy to prepare, but because of the large number of side reactions and the unclear structure of the products, related mechanisms have always been argued. From the perspective in this work, assuming that the CDs of our TEM (Fig. S6, ESI†) can comprehensively reflect the overall size, samples of b-, y-, and r-CDs with particle sizes of 3.97, 4.37,

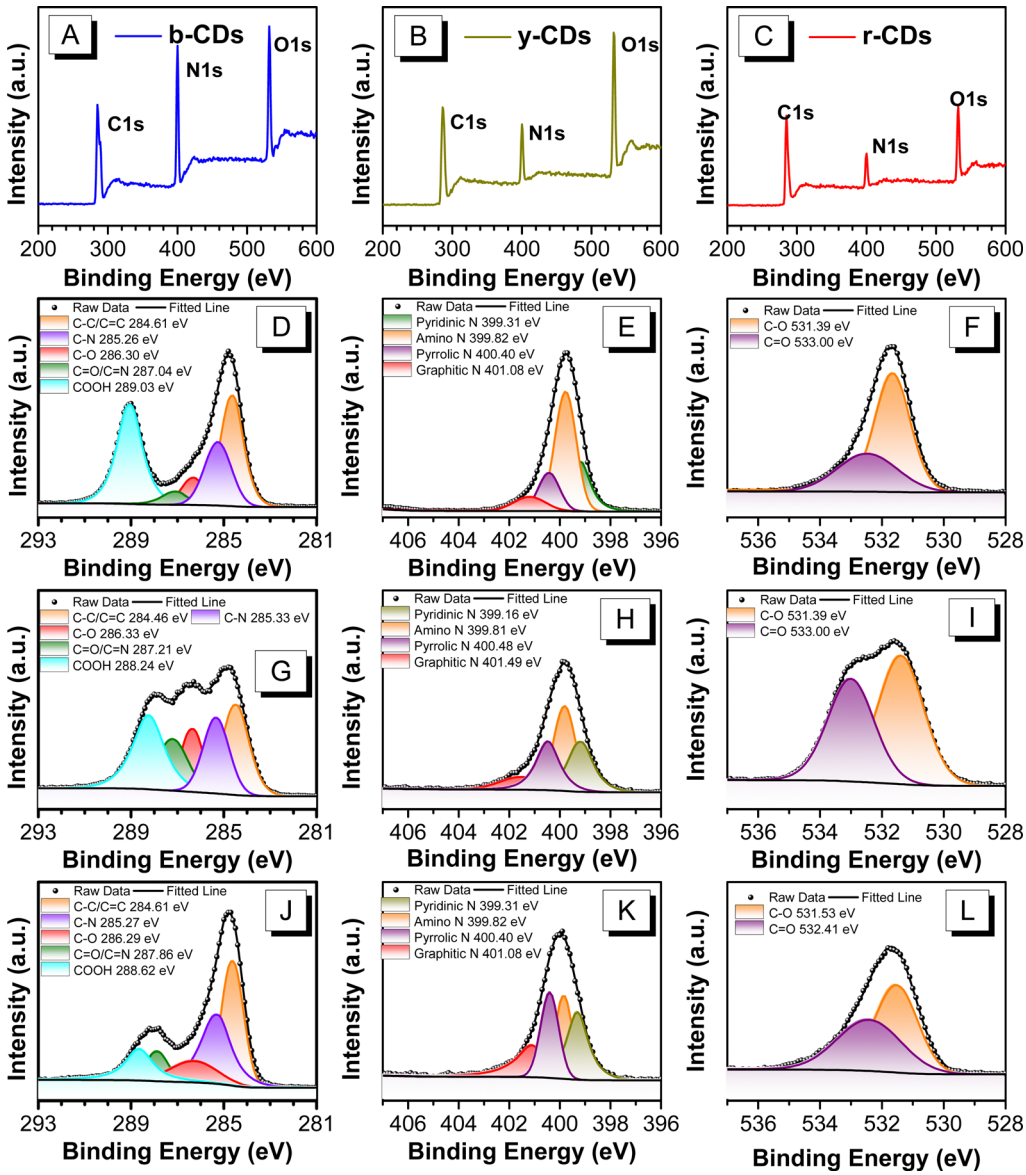

Fig. 2 XPS full scan spectra (A–C). C1s, N1s and O1s spectra of b-CDs (D–F), y-CDs (G–I) and r-CDs (J–L), respectively.

and 5.15 nm, respectively, can be seen. Therefore, particle size and surface state jointly affect fluorescence performance.

Latent fingerprint identification

In order to test the performance of the CD phosphor for LFP detection, several substrates were selected, including glass, printing paper, corrugated paper, wood (bare and uncoated), steel plate, plastic sheet and commercial labels (Fig. 3). Before LFP detection, we optimized the mass ratio between CDs and organosiloxane based on quantum yield. It was found that CD/organosiloxane with a mass ratio of 1 : 200 has the highest QY (the QY data have been given in the optical properties above). As shown in Fig. 3A–E, LFP can be clearly detected on all substrates. Due to the high contrast of the fluorescent signal, the ridge pattern of all samples (such as the bow, ring and thread of the level 1) can be clearly identified, which is clearer and more detailed than the stamp-pad ink commonly used in the office (Fig. 3B). It still performs well on the surface containing an interference surface, such as printing paper, corrugated paper, and commodity labels. However, the fluorescence os-b-CDs can be easily affected by the fluorescent brightener of printing paper, which results in lower resolution images, while yellow light and red light can obtain good image resolution (B–E). The features of the fingerprint are magnified in Fig. 3, including most of the ridge detail patterns related to level-1, level-2 and even level-3. It is well known that the features in the second level are randomly combined to give fingerprint uniqueness and invariance, which provides the most important identifiable information in fingerprint analysis. In Fig. 4(B1–5), (C1–5) and (D1–5), these characteristics are clearly observed and marked as bifurcation, island, termination, lake, whorl and short ridge. In general, when a specific defect and/or level 2 signal ambiguity happens, the level

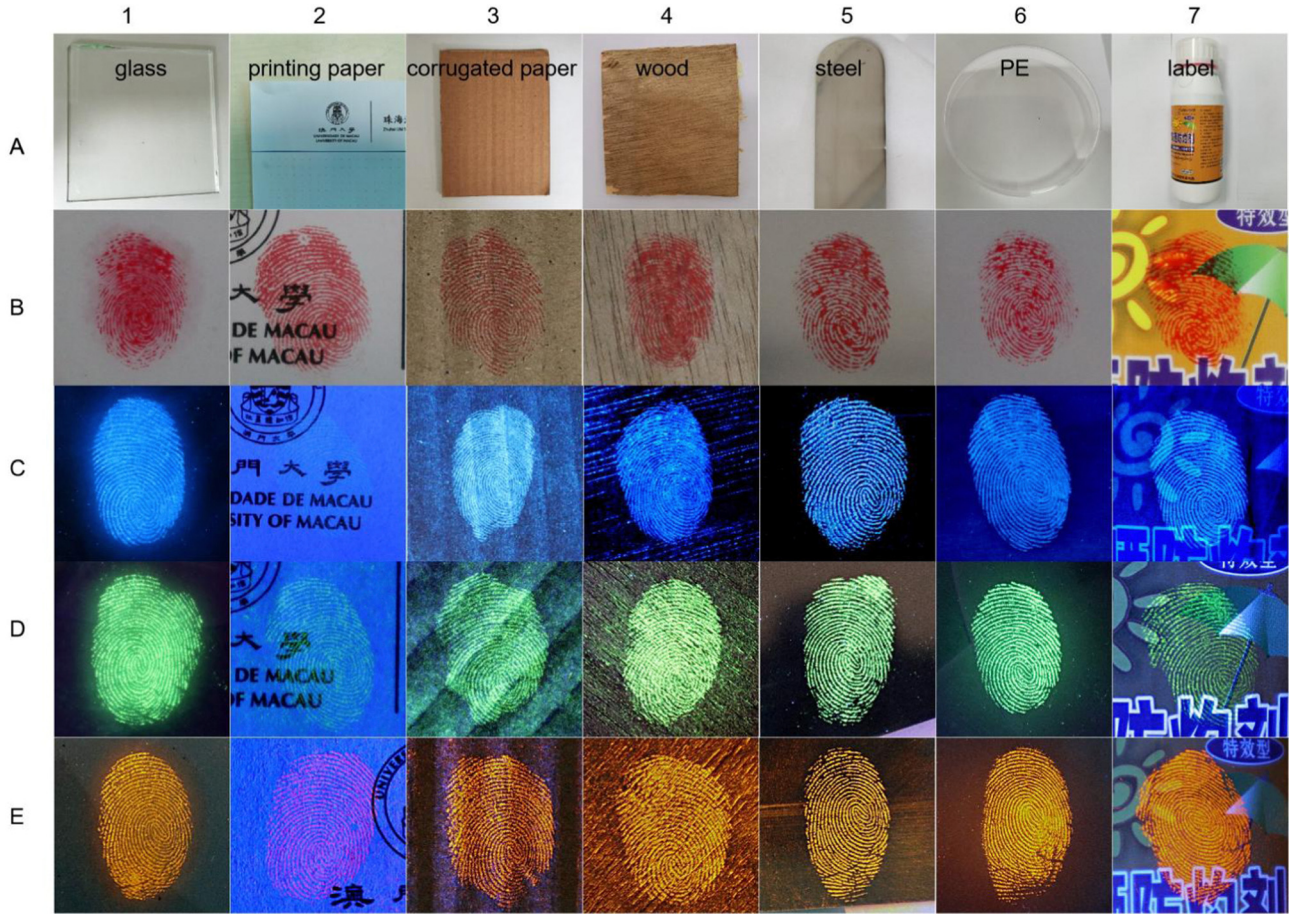

Fig. 3 Photographs of CD powder-stained fingerprints on glass sheet, printing paper, corrugated paper, wood, steel, PE (poly ethylen), and label, respectively. (A) Various substrates. (B) Stamp-pad ink-stained fingerprint. (C) os-b-CDs, (D) os-y-CDs and (E) os-r-CD stained fingerprints under a UV lamp.

3 features provide important reference information, although they cannot be used to identify LFPs alone. The scar found in Fig. 4D and sweat pores in Fig. 4C1 and D3 are examples of level 3 features. Comparing the gray value/distribution graph of os-b(y, r)-CDs and stamp-pad ink (Fig. 4A–D and Fig. S7–10, ESI†), it can be more clearly seen that the modified CD powder in this work has clear ridges and furrows, whereas these features are seriously lost in the fingerprint of stamp-pad ink. This fluorescent image is still bright and clear even after several weeks of storage. In the gray value distance curves of Fig. 4(B-6, C-6 and D-6), the distance between fingerprint ridges (furrow) can already be clearly displayed in any one-dimensional direction, which belongs to level 3 information. In contrast, the comparison curve (Fig. 4A2) shows the zigzag signal indicating significant signal loss. The gray value distance curves in Fig. 4B were drawn using ImageJ software.

Ion probe

Due to their excellent optical properties, CDs are often proposed as fluorescent probes.[64,65] Therefore, we evaluated its sensing capabilities towards various ions. As shown in Fig. S11 (ESI†), it can be seen that Cu^{2+}, Fe^{2+}, Fe^{3+} and AcO^- can quench the fluorescence. Due to the internal filter effect, the excitation and emission wavelengths of CDs are absorbed by the copper amine complex formed on the surface, so the quenching phenomenon will occur. After coordination with Fe^{3+}, the non-radiative transfer process from the excited electrons of CDs to the orbitals of metal ions can lead to fluorescence attenuation.[66] The quenching fluorescence of Cu^{2+}, Fe^{2+}, and Fe^{3+} ions is very common in the research report of the CD fluorescence probe, but the response to AcO^- is rare. Table 1 provides a comparison of the performance of the present probe with previous reports on fluorescent probes for AcO^-. In terms of their type (molecular structure), fluorescent response mode, working solution and limit of detection are given in Table 1. It can be clearly seen that it is difficult to find a carbon dot as a fluorescent probe for AcO^- detection. Compared with other sensors, the detection limit of this work is low and the working solution is water. The mechanism of the AcO^- probe may be attributed to the binding of the exposed amine and N=C to the AcO^- at the CD surface. As the concentration of AcO^- increases from 3×10^{-7} to 3×10^{-3} M, the fluorescence intensity of y-CD gradually extinguishes. Obviously, after adding 3 μM and 3 mM AcO^-, the fluorescence intensity decreases by more than 13% and 70%, respectively (Fig. 5). As the detection range of AcO^- is wide and the threshold is low, it fully proves the feasibility of AcO^- detection. It indicates that the quenching process is simple static quenching since the fluorescence attenuation data has no obvious change after adding AcO^-. It can infer

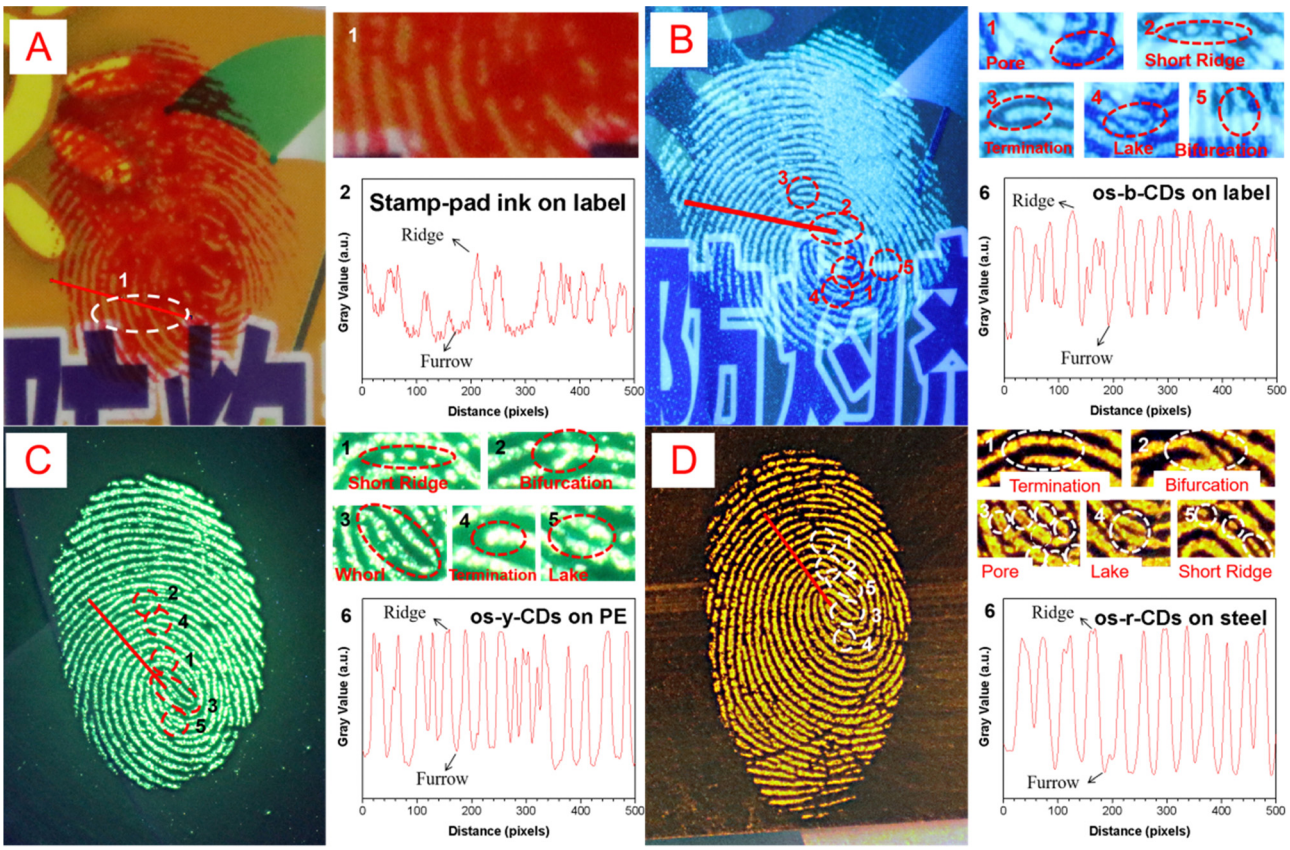

Fig. 4 (A) Stamp-pad ink stained on label, (B) os-b-CD stained on label, (C) os-y-CD stained on PE, and (D) os-r-CD stained on steel. The magnified images (B1–5), (C1–5) and (D1–5) show specific details, such as pore, termination, short ridge, lake, bifurcation, and whorl. The magnified images (A1) only show level 1 features.

Table 1 Comparison of some AcO^- fluorescence probes[49–63]

Ref.	Fluorescent probe type	Response mode	Solvent	Detection limit (M)
49	Schiff base	On	CH_3CN	1×10^{-6}
50 and 51	Trifluoroacetophenone derivative	On	—	8×10^{-7}
52	Schiff base	Off	—	4.3×10^{-7}
53	Thiourea based derivative	off	—	5.4×10^{-7}
54	Schiff base	On	DMSO	4.0×10^{-7}
55	Uranyl salophen	On	CH_3CN–H_2O	2.5×10^{-8}
56	Rhodamine 6G phenylurea	Off	CH_3CN–H_2O	1.8×10^{-7}
57	Naphthalene based derivative	On	CH_3CN	5.8×10^{-6}
58	Schiff bases	On	—	2.9×10^{-8}
59	Triazole Schiff bases	On	DMSO–H_2O	6.6×10^{-6}
60	Thio-urea based derivative	On	DMSO	1.5×10^{-7}
61	Schiff base	On	CH_3CN	6×10^{-7}
62	Schiff base	Ratiometric	DMSO	6×10^{-7}
63	Bis(triphenylphosphoniomethylene)anthracene dihexafluorophosphate	Off	DMSO	1.6×10^{-5}
This work	Carbon dot	Off	H_2O	3×10^{-7}

that the fluorescence of y-CDs was quenched by AcO^- due to the formation of non-fluorescent compounds that inhibit fluorescence emission.

Conclusions

To sum up, we developed a simple and convenient strategy of extraction and organosilicon encapsulation to separate CDs, and obtain fluorescent powder with multiple wavelengths. The CD powder was modified to improve the interaction with fingerprint residue, which was successfully used for multi-color imaging of LFPs. Notably, the multi-wavelength characteristic of CD powder can avoid interference on the substrate. The gray value curve data and level 3 characteristics from the magnified fluorescent photos indicate that the collected fingerprints have both high contrast and high sensitivity.

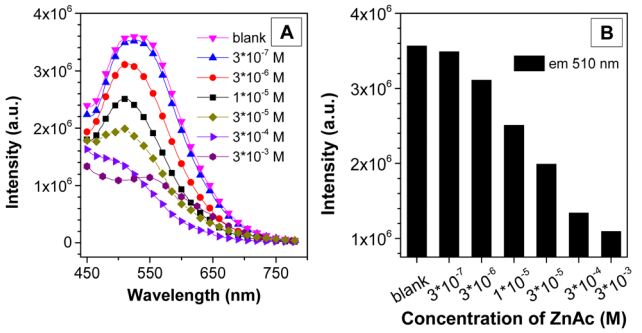

Fig. 5 (A) Emission spectra of y-CDs after different additions of AcO^-. (B) Emission intensity of y-CDs at 510 nm. CD solution concentration: 0.1 mg mL^{-1}.

The excellent performance on different substrates shows that the products of this work have wide applicability. Besides, a CD fluorescent probe capable of detecting AcO^- was prepared, with a low fluorescence response threshold (0.3 μM) and wide concentration range of response. The fluorescence response to AcO^- suggests that it is promising tool for AcO^- detection and fluorescence imaging in metabolic processes. In terms of industrial applications, two issues (mature regulatory mechanisms and mature industrial production processes) must be addressed first. Once these issues are settled, CDs will be rapidly applied to various aspects of society.

Author contributions

The study was designed by Guoxing Sun and executed by Tingzhong Li. The manuscript was written through contributions from all authors. All authors have given approval of the final version of the manuscript.

Conflicts of interest

There are no conflicts to declare.

Acknowledgements

This work was funded by the China Postdoctoral Science Foundation (2022M713666); the National Natural Science Foundation of China, Excellent Young Scientists Fund (HK&Macau) (file no. 52122001); Shenzhen-Hong Kong-Macao Science and Technology Plan (c) (file no. SGDX2020110309360301); The Science and Technology Development Fund, Macau SAR (file no. 0138/2020/A3); and the Science and Technological Bureau of Guangzhou Huangpu District (file no. 2021GH09).

References

1 D. Fernandes, M. J. Krysmann and A. Kelarakis, *Chem. Commun.*, 2015, **51**, 4902–4905.
2 S. Li, H. Zheng, L. Ding, X. Xiao, Y. Niu, Y. Tang, Z. Liu, W. Zhang, Y. Zhou and Q. Xu, *J. Mater. Chem. C*, 2022, **10**, 14282–14287.
3 J. Wang, F. Wang, C. Wang, Z. Liu and X. Liu, *Angew. Chem., Int. Ed.*, 2011, **50**, 10369–10372.
4 K. Shwetabh, S. K. Maurya, A. Banerjee, R. Poddar and K. Kumar, *New J. Chem.*, 2022, **46**, 21950–21961.
5 O. S. Wolfbeis, *Chem. Soc. Rev.*, 2015, **44**, 4743–4768.
6 S. Cheng, A. Li, X. Pan, H. Wang, C. Zhang, J. Li and X. Qi, *Anal. Bioanal. Chem.*, 2021, **413**, 4441–4450.
7 Y. Wang, C. Li, H. Qu, C. Fan, P. Zhao, R. Tian and M. Zhu, *J. Am. Chem. Soc.*, 2020, **142**, 7497–7505.
8 Y. Liu, J. Wei, X. Yan, M. Zhao, C. Guo and Q. Xu, *Chin. Chem. Lett.*, 2021, **32**, 861–865.
9 F. Yuan, Z. Wang, X. Li, Y. Li, Z. Tan, L. Fan and S. Yang, *Adv. Mater.*, 2017, **29**, 1604436.
10 T. Li, Y. Ning, J. Pang, L. Chen, F. Zhang and F. Chai, *New J. Chem.*, 2023, **47**, 147–155.
11 P. Lesani, S. M. Ardekani, A. Dehghani, M. Hassan and V. G. Gomes, *Sens. Actuators, B*, 2019, **285**, 145–155.
12 P. Lesani, G. Singh, Z. Lu, M. Mirkhalaf, E. J. New and H. Zreiqat, *Chem. Eng. J.*, 2022, **433**, 133668.
13 H. Wang, M. Zhang, Y. Song, H. Li, H. Huang, M. Shao, Y. Liu and Z. Kang, *Carbon*, 2018, **136**, 94–102.
14 Y. B. Song, S. J. Zhu and B. Yang, *RSC Adv.*, 2014, **4**, 27184–27200.
15 P. Lesani, A. H. Mohamad Hadi, Z. Lu, S. Palomba, E. J. New and H. Zreiqat, *Commun. Mater.*, 2021, **2**, 108.
16 P. Lesani, G. Singh, C. M. Viray, Y. Ramaswamy, D. M. Zhu, P. Kingshott, Z. Lu and H. Zreiqat, *ACS Appl. Mater. Interfaces*, 2020, **12**, 18395–18406.
17 X. Wang, Y. Yuan, Y. Sun, X. Liu, M. Ma, R. Zhang and F. Shi, *RSC Adv.*, 2022, **12**, 27199–27205.
18 F. Li, L. Tang, Y. Liu and J. Shao, *Opt. Mater.*, 2022, **128**, 112356.
19 D. Zhou, D. Li, P. Jing, Y. Zhai, D. Shen, S. Qu and A. L. Rogach, *Chem. Mat.*, 2017, **29**, 1779–1787.
20 H. Tan, G. Gong, S. Xie, Y. Song, C. Zhang, N. Li, D. Zhang, L. Xu, J. Xu and J. Zheng, *Langmuir*, 2019, **35**, 11503–11511.
21 J. Li, Z. Jiao, P. Zhang, X. Wan, C. Song, Z. Guo, X. Huang and B. Z. Tang, *Mater. Chem. Front.*, 2020, **4**, 2131–2136.
22 A. Sekar, R. Vadivel, R. G. Munuswamy and R. Yadav, *New J. Chem.*, 2021, **45**, 17447–17460.
23 R. Wang, Z. Huang, L. Ding, F. Yang and D. Peng, *ACS Appl. Nano Mater.*, 2022, **5**, 2214–2221.
24 J. L. Wang, F. Zhang, Y. L. Wang, Y. Z. Yang and X. G. Liu, *Carbon*, 2018, **126**, 426–436.
25 Z. Xie, F. Wang and C. Liu, *Adv. Mater.*, 2012, **24**, 1716–1721.
26 B. Jiang, Y. Yu, X. Guo, Z. Ding, B. Zhou, H. Liang and X. Shen, *Carbon*, 2018, **128**, 12–20.
27 Y. Zhang, P. Zhuo, H. Yin, Y. Fan, J. Zhang, X. Liu and Z. Chen, *ACS Appl. Mater. Interfaces*, 2019, **11**, 24395–24403.
28 G. Hu, Y. Wang, S. Zhang, H. Ding, Z. Zhou, J. Wei, X. Li and H. Xiong, *Carbon*, 2023, **203**, 1–10.
29 M. Shao, Q. Yu, N. Jing, Y. Cheng, D. Wang, Y. Wang and J. Xu, *Lab Chip*, 2019, **19**, 3974–3978.
30 J. Shao, S. Zhu, H. Liu, Y. Song, S. Tao and B. Yang, *Adv. Sci.*, 2017, **4**, 1700395.

31 K. Jiang, S. Sun, L. Zhang, Y. Lu, A. Wu, C. Cai and H. Lin, *Angew. Chem., Int. Ed.*, 2015, **54**, 5360–5363.
32 F. Huo, Y. Liu, M. Zhu, E. Gao, B. Zhao and X. Yang, *ACS Appl. Mater. Interfaces*, 2019, **11**, 27259–27268.
33 C. Shen, Q. Lou, C. Lv, J. Zang, S. Qu, L. Dong and C. Shan, *Adv. Sci.*, 2019, **6**, 1802331.
34 P. Lesani, Z. Lu, G. Singh, M. Mursi, M. Mirkhalaf, E. J. New and H. Zreiqat, *Nanoscale*, 2021, **13**, 11138–11149.
35 D. Zhao, W. Ma and X. Xiao, *Nanomaterials*, 2018, **8**, 612.
36 H. J. Wang, W. Y. Hou, T. T. Yu, H. L. Chen and Q. Q. Zhang, *Dyes Pigm.*, 2019, **170**, 107623.
37 W. Chan, J. D. Zhou, L. L. Lu and Q. J. Song, *Part. Part. Syst. Charact.*, 2018, **35**, 1700387.
38 J. Chen, J. S. Wei, P. Zhang, X. Q. Niu, W. Zhao, Z. Y. Zhu, H. Ding and H. M. Xiong, *ACS Appl. Mater. Interfaces*, 2017, **9**, 18429–18433.
39 A. Ansari, K. Aldajani, A. AlHazaa and H. Albrithen, *Coord. Chem. Rev.*, 2022, 462.
40 Z. Qin, M. Wen, J. Bai, J. Cui, R. Miao, X. Zhang, Q. Zhang, R. Zhang and X. Du, *New J. Chem.*, 2021, **45**, 11596–11606.
41 T. Gunnlaugsson, P. E. Kruger, P. Jensen, J. Tierney, H. D. P. Ali and G. M. Hussey, *J. Org. Chem.*, 2005, **70**, 10875–10878.
42 A. Davenport, E. J. Will and A. M. Davison, *Nephron*, 2008, **59**, 461–465.
43 X. Shang and X. Xu, *BioSystems*, 2009, **96**, 165–171.
44 S. Qu, D. Zhou, D. Li, W. Ji, P. Jing, D. Han, L. Liu, H. Zeng and D. Shen, *Adv. Mater.*, 2016, **28**, 3516–3521.
45 R. Dong, J. Wu, T. You and W. Cao, *Materials*, 2021, **15**, 30.
46 S. Lei, W. Cao, Z. Fu and L. Xu, *J. Appl. Polym. Sci.*, 2016, **133**, 43890.
47 K. K. Chan, C. Yang, Y. Chien, N. Panwar and K. Yong, *New J. Chem.*, 2019, **43**, 4734–4744.
48 S. Zhu, Q. Meng, L. Wang, J. Zhang, Y. Song, H. Jin, K. Zhang, H. Sun, H. Wang and B. Yang, *Angew. Chem., Int. Ed.*, 2013, **52**, 3953–3957.
49 B. Biswas, *J. Indian Chem. Soc.*, 2017, **94**, 811–818.
50 D. Ryu, E. Park, D. Kim, S. Yan, J. Y. Lee, B. Chang and K. H. Ahn, *J. Am. Chem. Soc.*, 2008, **130**, 2394–2395.
51 D. Kim and K. H. Ahn, *J. Org. Chem.*, 2008, **73**, 6831–6834.
52 V. K. Gupta, N. Mergu, L. K. Kumawat and A. K. Singh, *Talanta*, 2015, **144**, 80–89.
53 G. Vinithra, S. Suganya and S. Velmathi, *Tetrahedron Lett.*, 2013, **54**, 5612–5615.
54 Q. Lin, X. Liu, T. Wei and Y. Zhang, *Sens. Actuators, B*, 2014, **190**, 459–463.
55 M. Hosseini, M. R. Ganjali, B. Veismohammadi, F. Faridbod, S. D. Abkenar and M. Salavati Niasari, *Luminescence*, 2012, **27**, 341–345.
56 Z. Q. Hu, X. M. Wang, Y. C. Feng, L. Ding, M. Li and C. S. Lin, *Chem. Commun.*, 2011, **47**, 1622–1624.
57 S. Goswami, A. K. Das, D. Sen, K. Aich, H. Fun and C. K. Quah, *Tetrahedron Lett.*, 2012, **53**, 4819–4823.
58 N. Borah, S. De, A. Gogoi and G. Das, *New J. Chem.*, 2020, **44**, 18703–18713.
59 A. A. Balakit, S. Q. Makki, Y. Sert, F. Ucun, M. B. Alshammari, P. Thordarson and G. A. El-Hiti, *Supramol. Chem.*, 2020, **32**, 519–526.
60 S. K. Patra, B. Sen, S. K. Sheet, B. Banerjee, N. Saha and S. Khatua, *Inorg. Chim. Acta*, 2019, **492**, 119–130.
61 S. Goswami, S. Maity, A. K. Das and A. C. Maity, *Tetrahedron Lett.*, 2013, **54**, 6631–6634.
62 G. Liu and J. Shao, *J. Fluoresc.*, 2012, **22**, 397–401.
63 W. Huang, H. Lin and H. Lin, *Sens. Actuators, B*, 2011, **153**, 404–408.
64 J. Li, G. Zuo, X. Pan, W. Wei, X. Qi, T. Su and W. Dong, *Luminescence*, 2018, **33**, 243–248.
65 J. Li, G. Zuo, X. Qi, W. Wei, X. Pan, T. Su, J. Zhang and W. Dong, *Mater. Sci. Eng., C*, 2017, **77**, 508–512.
66 M. R. Hormozi-Nezhad and M. Taghipour, *Anal. Methods*, 2016, **8**, 4064–4068.